J. Fluid Mech. (1975), *vol.* 71, *part* 3, *pp.* 563–575
Printed in Great Britain

An experimental study of the instability of a stably stratified free shear layer

By YU-HWA WANG

Coastal and Oceanographic Engineering Laboratory, University of Florida, Gainesville

(Received 19 September 1974)

A stably stratified free shear layer is created in a continuously circulating water channel in the laboratory. Two streams of salt water of different concentrations are brought together at the entrance to the open channel and a layered uniform flow field with a distinct sharp interface is produced in the test section. The maximum density difference between the two layers is $\Delta\rho_{\max} = 0{\cdot}0065\rho_w$, where ρ_w is the density of water. The velocity of each layer can be adjusted at will to create free shear across the interface. At the end of the open channel, a mechanical device to separate the layers for recirculation is provided. The resulting flow field has a viscous region approximately 15 times larger than the scale of the salinity diffusion layer. Visual observations are made with hydrogen bubbles and dye traces. Interfacial waves are initiated by artificial excitation. The perturbation frequencies range from 0·476 to 10·40 Hz. The measured wavelengths range from 0·46 to 3·02 cm. Damped waves as well as growing waves are observed at various exciting frequencies. Velocity profiles and instantaneous velocities are measured by a hot-film anemometer designed for use in salt water. Experimental values of the Richardson number, the dominant parameter characterizing the instability process, range from 1·23 to 14·45. The stability boundary is determined experimentally. Comparisons with Hazel's numerical results and the earlier results of Scotti & Corcos for low values of the Richardson number are also made.

1. Introduction

Since Taylor (1931) laid the theoretical foundations, a large number of authors have studied the stability of stratified shear flows and the resulting turbulence. Miles (1961) showed that a sufficient condition for stability is that the local Richardson number be equal to or greater than $\frac{1}{4}$ everywhere in the flow, and that the stability boundary consists of singular neutral modes. Howard (1961) proved that an unstable eigenvalue of the complex phase speed in the Taylor–Goldstein equation (Thorpe 1969) must lie inside the semicircle in the upper half-plane of the complex eigenvelocity which has the range of U as its diameter. Drazin & Howard (1966) summarized many examples of stability for special velocity and density distributions. Hazel (1972) showed the stability characteristics to be influenced by boundary conditions and the ratio of the velocity to the thickness of the density interface.

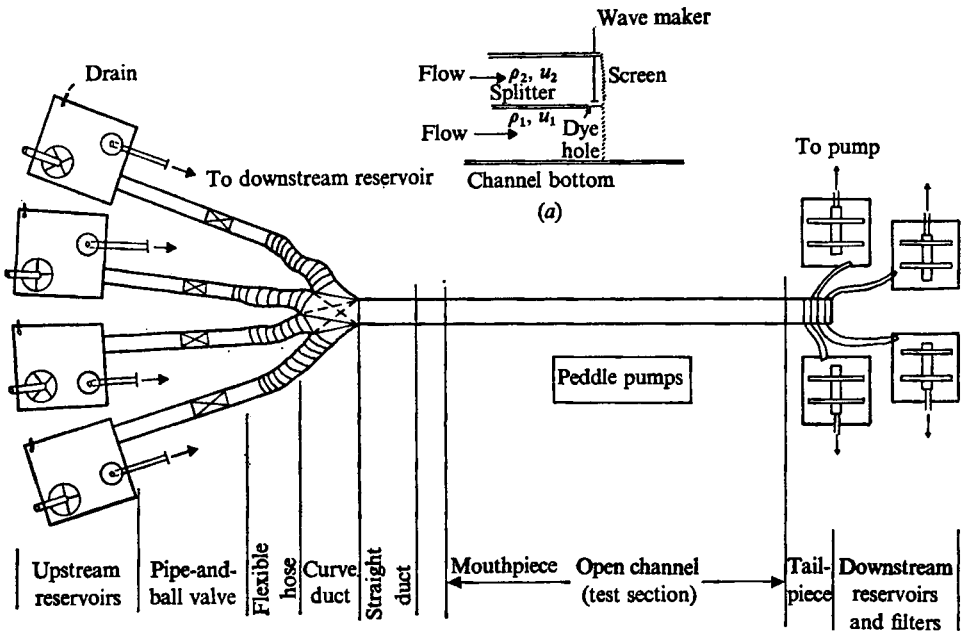

FIGURE 1. Schematic diagram of stratified recirculating water channel. (*a*) Mouthpiece.

There are only a few published experiments designed to confirm these various analyses. Scotti & Corcos (1972) studied a density-stratified free shear flow, attained in a wind tunnel by merging two streams of air of different temperatures, over a Richardson number range of 0·07–0·76. They observed instabilities to occur for Richardson numbers less than roughly $\frac{1}{4}$. Thorpe (1971) attained an accelerating, stratified, free shear flow by tilting a long rectangular tube containing fluids of different densities and subsequently developed a number of interesting phenomenological pictures of instability. In the current experiment, emphasis has been placed on experimental determination of stability boundaries.

2. Experimental set-up and procedure

Apparatus

The apparatus employed in this investigation for the production of a recirculating stratified flow is shown schematically in figure 1. The test channel is supplied from upstream reservoirs providing water of various salt concentrations. A constant head is maintained in each reservoir by an outlet cone emptying into the corresponding downstream reservoir and the flow rate in the channel is controlled by valves in the outlet section of each upstream reservoir. The flows upstream of the mouthpiece are smoothed by fine silk screens and a bundle of fine thin-walled glass tubes. The mouthpiece has a thin horizontal splitter plate separating the fluids of differing densiti es and leads dire ctly into the $10{\cdot}16 \times 10{\cdot}16 \times 182$ cm

long open channel test section. The flow may be observed through the Plexiglas sides of the channel. At the end of the open channel, the flow is partitioned into the components of differing densities through a 90° elbow tailpiece and discharged into the appropriate downstream reservoirs. The downstream reservoirs have filtering systems consisting of nylon screens. Diatomaceous earth added to the water attaches to the screens and further refines the filtering process. The water is pumped directly from the downstream to the upstream reservoirs.

The interface between the layers is sharp and distinctive, and no mixing is observed except on the molecular scale. The effectiveness of the tailpiece can be evaluated by observing the mixing process as evidenced by changes in the densities. An estimate indicates that the density difference changes by 6 % in the time required to move the entire volume of liquid through the system once. During a run of 17 h, the density difference changes by 30·8 %; this drift in the densities has been accounted for in the computations. The background turbulence, defined as the ratio u'/U of the fluctuating velocity u' to the mean velocity U, is found to be 1·7 % for $U = 2{\cdot}54$ cm/s.

Generation of shear and perturbation

The shear between the fluid strata is controlled through adjustment of the valves upstream of the test section; samples of the various degrees of shear attained appear in figures 2 and 3 (plate 1). Perturbations are introduced into the flow by a $0{\cdot}48 \times 0{\cdot}025$ cm ribbon stretched across the mouthpiece just above the interface between the fluid strata and behind a silk screen (figure 1*a*). The ribbon can be driven at between 0·476 and 10·4 Hz with an amplitude of approximately 0·06 cm. Wakes from the splitter plate and the ribbon are effectively eliminated by the silk screen.

Instrumentation carriage

The instrument platform, sliding on two bars fixed longitudinally to the channel, can place probes anywhere in the channel by means of a motorized drive. The vertical and transverse positions of the probes can be read directly to an accuracy of approximately 0·0025 cm from a calibrated digital register or recorded from an analog voltage output.

Velocity sensor and stratification

The hot-film probe used in this investigation, a standard product of Thermo-Systems Inc. designed for use in salt water, has as its sensing element a quartz-coated cylinder 0·0051 cm in diameter by 0·10 cm long. The probe was calibrated by the 'shedding frequency' method (Roshko 1954; Fabula 1967; Tritton 1971), employing a vortex-shedding cylinder of diameter $d = 0{\cdot}108$ cm suitable for the velocity range of this study. With the sensor placed $3d$ below and $6d$ behind the cylinder, where the fluid velocity is very nearly the free-stream velocity (Kovasznay 1949), the output signal was a distinctively sinuous curve, facilitating frequency counting.

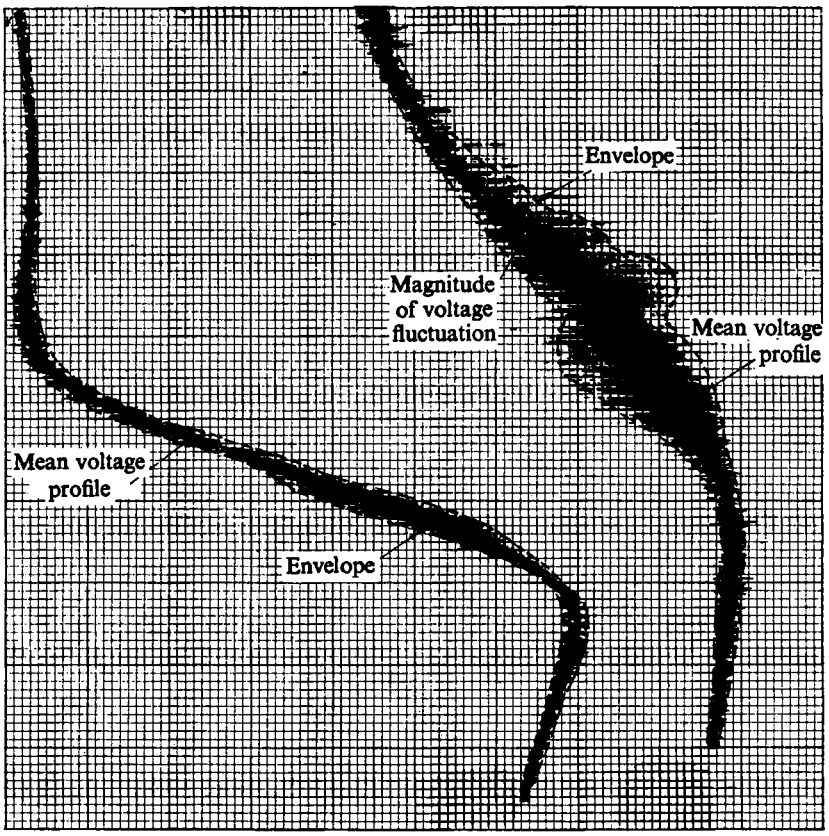

FIGURE 4. Voltage output of a hot-film sensor near the interface of a two-layered stratified flow.

The heat-transfer properties of the hot-film probe are given by Hinze (1959, p. 76):

$$Nu = 0{\cdot}42Pr^{0{\cdot}2} + 0{\cdot}57Pr^{0{\cdot}33}Re^{0{\cdot}5},$$

where Nu is the Nusselt number, Pr is the Prandtl number and Re is the Reynolds number. Since the Prandtl number and the Reynolds number vary as the density of the medium, and since the variation of density in these experiments was of the order of $\frac{1}{2}\%$ ($\Delta\rho_{\max} = \rho_1 - \rho_2 = 0{\cdot}0065\rho_w$), the calibration curve of the probe can be considered unchanged between strata.

Conductivity and velocity measurements

A single electrode conductivity probe similar in design to that of Gibson & Schwarz (1963) was used for density measurements. Difficulty was encountered with spatial resolution, a smoothly varying density being recorded as the probe was traversed across the practically discontinuous interface. Because of this problem, the conductivity probe was used only as a diagnostic tool in the present investigation.

The velocity profiles were measured by driving the hot-film sensor across the interface at a speed of approximately 0·0025 cm/s. A sample voltage record from the hot-film anemometer is shown in figure 4. Horizontal line segments between the envelopes of the voltage fluctuations represent the magnitudes of the fluctuations and the locus of the midpoints of these horizontal segments represents the mean voltage profile. The mean velocity profiles were obtained from the mean voltage profiles through the speed–voltage calibration curve. The fluctuating voltage e' was converted to the fluctuating velocity u' according to Hinze (1959, p. 117):

$$u' = 4e'\bar{E}\sqrt{U}/BR_w(R_w - R_g),$$

where R_w is the actual electrical resistance of the hot film, R_g is its resistance at the ambient temperature of the fluid, B is the slope of the velocity calibration curve, $\bar{E}$ is the mean voltage and U is the mean velocity. Since, as has been noted, the effects of the stratification on the probe calibration are negligible, the above equation may be used with confidence.

The extent of the perturbed flow was made visible by dyeing the lower stratum (see figure 2). At all perturbation frequencies, measurements were made at stations downstream from the ribbon only as far as the flow was visibly disturbed. Typical spacings between stations are 1·27 cm near the mouthpiece, 2·54 cm for moderate distances from the mouthpiece and 5·08 cm far downstream.

3. Results and discussion

Nature of the stability

The interface was made visible by dyeing the lower stratum. With no artificial excitation and a small velocity difference ΔU between strata (either $U_1 > U_2$ or $U_1 < U_2$), the interface is smooth and undisturbed over the entire length of the channel. For slightly larger ΔU, ripples are observed on the interface from about 8 to 16 cm downstream from the splitter plate, beyond which the flow is again undisturbed. As ΔU is further increased, the waves increase in amplitude and propagate further downstream.

At this point, the wave forms depart from two-dimensionality, spanwise irregularities of smaller amplitude and wavelength than the streamwise waves being observed. This is most readily seen from the tendency of the normally straight troughs and crests of the streamwise waves to become crooked as the waves propagate downstream. The irregularities disappear and the waves resume a two-dimensional character as ΔU is yet further increased. When ΔU becomes sufficiently large, the waves break within two or three wavelengths of the mouthpiece (figure 2), and finally turbulent mixing occurs at the interface.

While variation of ΔU leads to interesting qualitative descriptions of the nature of the stability of the flow, it is difficult to extract from such observations useful quantitative data concerning the stability boundaries. For this purpose, artificial excitation similar to that of Klebanoff, Tidstrom & Sargent (1962) is used: ΔU is adjusted such that intermittent wrinkling appears on the undisturbed interface (see figure 3); the perturbation ribbon is then driven at the

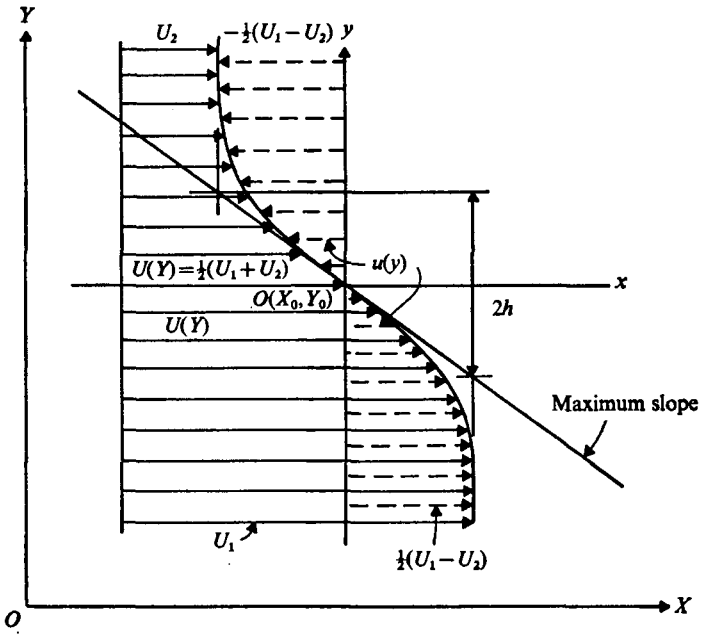

FIGURE 6. Definition sketch of the velocity profile.

desired frequency and measurements are made at downstream positions. A typical example of interfacial waves with artificial excitation is shown in figure 5 (plate 1).

With artificial perturbation of the system, no disturbances of the flow are observed until the perturbation frequency is increased to 1·85 Hz. At this point, ripples begin to form at the interface. As the perturbation frequency is increased, the ripples grow in amplitude and propagate further downstream until a maximum amplitude is reached, for a perturbation frequency of 3·61–4·88 Hz; these waves travel the entire length of the channel with wavelengths elongated and crests flattened far downstream. With further increases in the perturbation frequency, the waves decrease in amplitude and propagate a shorter distance downstream.

Characteristics of the velocity profile

Figure 6 is a definition sketch of the co-ordinate system. The X, Y co-ordinates are attached to the laboratory frame and x, y co-ordinates are attached to the flow such that $y = 0$ is at the interface and such that $u(y = 0) = 0$. The shear-layer thickness $2h$ is defined by

$$[\partial u/\partial y]_{y=0} = \Delta U/h.$$

In the vicinity of the interface, there is a region approximately 1 cm deep in which relatively large velocity fluctuations occur (see figure 4). These fluctuations are produced by the perturbing ribbon, are regular in frequency and can thus in no way be construed as turbulence. Their growth and decay are presented

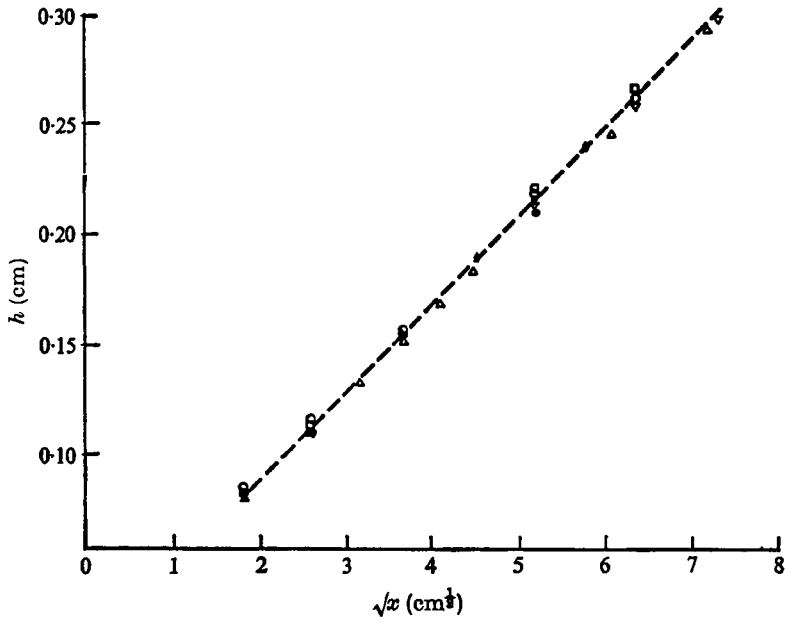

FIGURE 7. Shear-layer thickness as a function of $\sqrt{x}$.

	△	▽	●	○	□	◆
F (Hz)	1·85	3·05	4·88	7·34	8·60	10·40

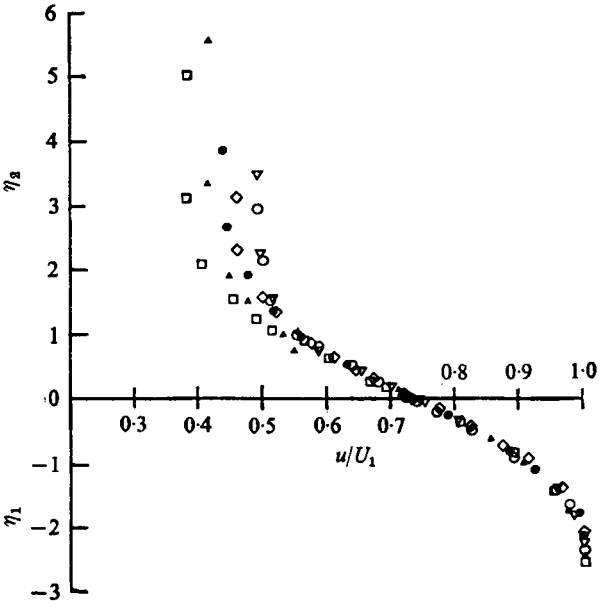

FIGURE 8. Non-dimensional mean velocity profile at different downstream positions.

	□	▲	●	◇	▽	○
x (cm)	1·27	2·54	5·08	7·62	10·16	12·70

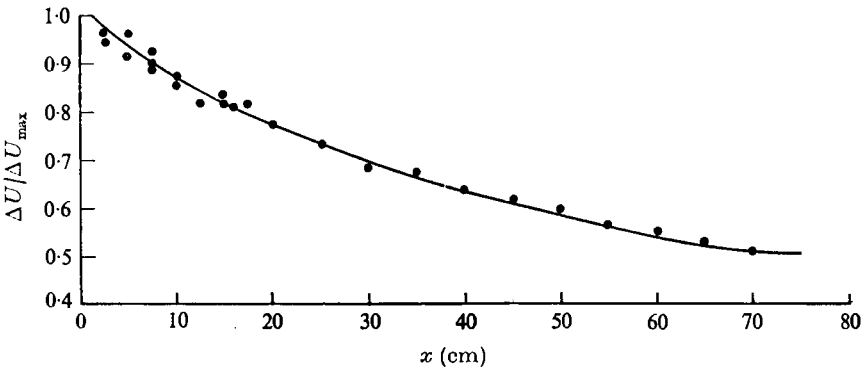

FIGURE 9. Variation of total velocity difference with downstream position.

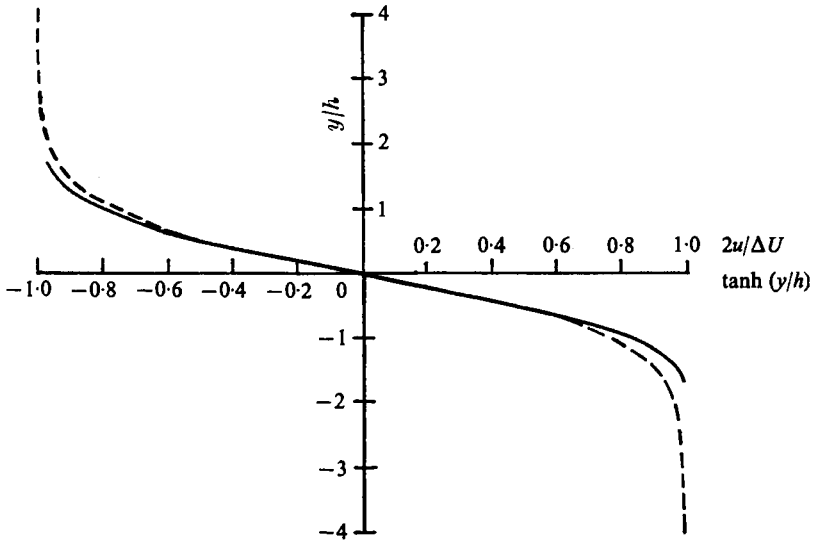

FIGURE 10. Comparison between measured velocity profile $2u/\Delta U$ (solid line) and hyperbolic-tangent profile (dashed line).

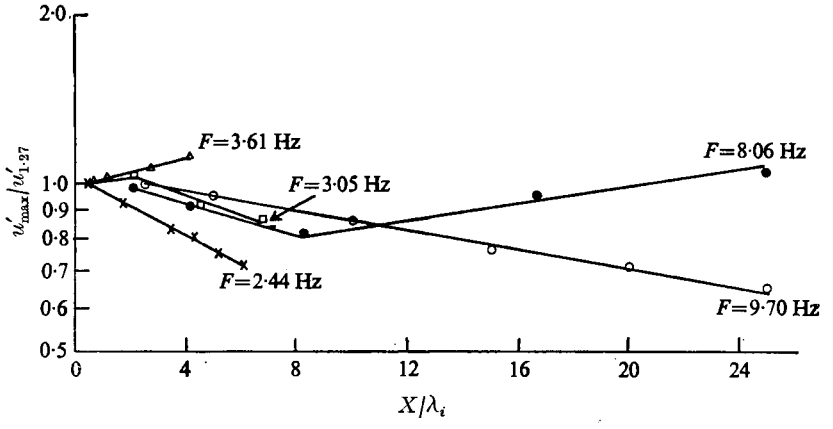

FIGURE 11. Decay and growth of maximum u' with downstream position. λ_i = initial wavelength, $u'_{1·27}$ = value of u'_{max} at x = 1·27 cm.

in figure 11. That the background turbulence intensity u'/U drops to 1·7% outside this region and that the shear layer is described by a strictly laminar growth law (figure 7) demonstrates the laminar nature of the flow.

In non-turbulent flows, the velocity profile near the interface is expected to have laminar similarity. Thus a single independent variable should describe adequately the velocity profile at any downstream position:

$$V = V(\eta),$$

where V is the non-dimensional mean velocity, $V = u/U_1$, and η is the similarity parameter,

$$\eta = \begin{cases} \eta_1 = y(U_1/\nu_1 x)^{\frac{1}{2}} & \text{below the interface,} \\ \eta_2 = y(U_2/\nu_2 x)^{\frac{1}{2}} & \text{above the interface,} \end{cases}$$

U_1 and U_2 being the maximum mean velocities of the lower and upper strata and ν_1 and ν_2 their kinematic viscosities. The validity of this relationship is demonstrated in figure 7, where h is seen to vary as $\sqrt{x}$, and in figure 8, where the velocity profiles at various stations are seen to be similar when plotted *vs.* the similarity parameter η. (Since U_2 changes somewhat with increasing x, the curves in figure 8 approach different asymptotes for increasing η. This effect is reflected in a decrease in ΔU and is presented graphically in figure 9, where $\Delta U/\Delta U_{\max}$ is plotted *vs.* downstream position.)

In order for the results of this investigation to be directly compared with Hazel's analysis, it is necessary for the mean velocity profile to vary as the hyperbolic tangent of y/h. In figure 10, the velocity distribution is compared with the hyperbolic-tangent profile

$$2u/\Delta U = \tanh y/h$$

and the agreement is found to be good in the vicinity of the interface. Waves at the interface are taken to be stable or unstable according to whether the velocity fluctuations u' decay or grow with downstream distance. The maximum values of u' for various perturbation frequencies and downstream positions are plotted in figure 11. It is interesting to note that, for $F = 3{\cdot}05\,\text{Hz}$, u' grows initially and then decays, while for $F = 8{\cdot}60\,\text{Hz}$, u' decays initially and then starts to grow.

Determination of density gradients

Since the single electrode conductivity probe has poor spatial resolution, the density profile near the interface must be determined through the diffusion equation

$$u\frac{\partial \xi}{\partial x} + v\frac{\partial \xi}{\partial x} = D\frac{\partial^2 \xi}{\partial y^2},$$

where ξ is the concentration and D is the diffusion coefficient. The field velocities u and v in the shear layer are taken from Lock's (1951) approximate analysis of parallel laminar flow of liquids of differing physical properties:

$$u = U_1[C_{\tau 0}\eta + (u_0/U_1)], \quad v = \tfrac{1}{4}U_1 C_{\tau 0}\eta^2 (\nu_1/U_1 x)^{\frac{1}{2}},$$

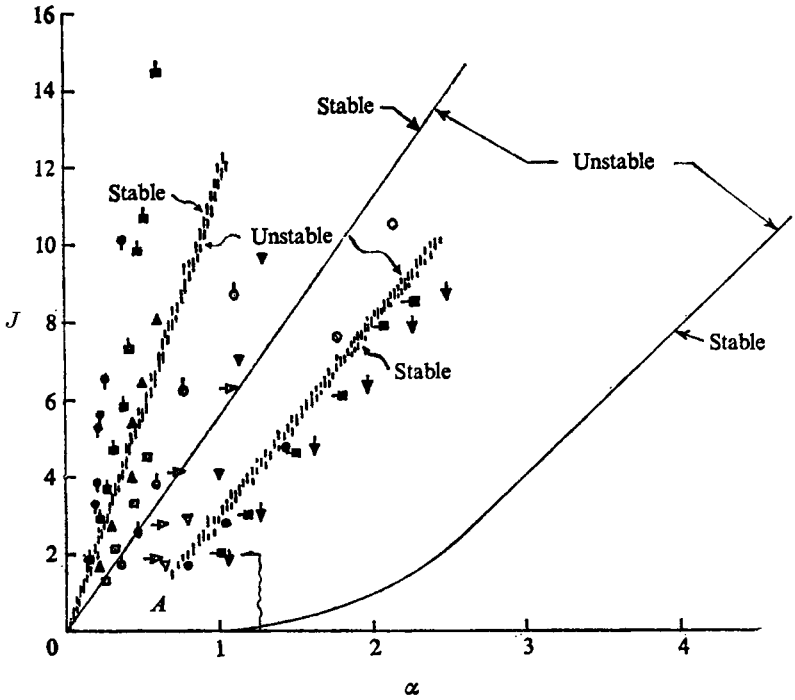

FIGURE 12. Stability characteristics showing regions of damped and growing waves and the stability boundary. Hatched lines indicate experimentally determined stability boundary for $10 < R < 19$. Solid lines are from Hazel's (1972) figure 8(*a*) for $R = 5$. Region A is shown enlarged in figure 13.

where u_0 is the interface velocity, C_{f0} is the friction coefficient and η is the similarity parameter. When the diffusion equation is integrated across the shear layer with the above velocity distribution, it is found that, to a good degree of approximation, the density profile varies as the hyperbolic tangent of the vertical position:

$$\rho = \rho_1 \exp\left[-(\sigma/R)\tanh(Ry)\right],$$

where
$$\sigma = -\frac{\rho_1-\rho_2}{\rho_1+\rho_2} h(x)\,(u_0/\pi Dx)^{\frac{1}{2}}, \quad R = 2\sigma/\ln(\rho_1/\rho_2).$$

Since the measured u_0 varies somewhat with x, the value of σ varies from 0·61 to 0·35 and that of R from 10 to 19. With the above expression for the density profile, the local Richardson number at $y = 0$ is

$$Ri|_{y=0} = J = \left.\frac{(-g/\rho)\,\partial\rho/\partial y}{(\partial u/\partial y)^2}\right|_{y=0} = \frac{g\sigma/h}{(\Delta U/2h)^2} = \frac{4g\sigma h}{\Delta U^2},$$

where g is the acceleration due to gravity.

The stability boundary

For each interfacial perturbation frequency, the local Richardson number J and the dimensionless wavenumber $\alpha = 2\pi h/\lambda$ were measured at downstream

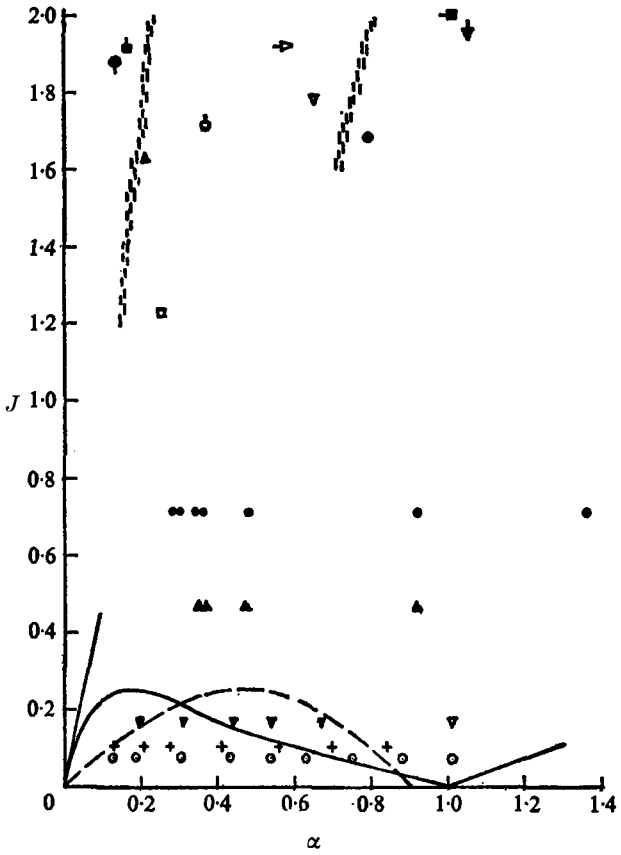

FIGURE 13. Stability characteristics at low values of J. Open symbols indicate growth and solid symbols decay. Data points below $J = 0{\cdot}8$ are from Scotti & Corcos (1972). Data points above $J = 0{\cdot}8$ are from this investigation. The solid lines are the neutral curve and stability boundary for hyperbolic-tangent profiles (Hazel 1972). The dashed line is the neutral curve for error-function profiles (Hazel 1972).

stations. A plot of J *vs.* α is presented in figure 12, where each symbol represents a perturbation frequency. The open symbols indicate unstable (growing) waves while the solid symbols indicate stable (diminishing) waves. The vertical hatching in figure 12 separates the stable and unstable region of the J, α plane. The solid lines are the numerical stability boundary of Hazel (1972, figure 8*a*) for $R = 5$.

It is interesting to note that, at a perturbation frequency of 3·05 Hz, initially unstable waves become stable as they travel downstream. This is reflected in figure 12 in that the triangles, representing a perturbation frequency of 3·05 Hz, pass from the unstable region to the stable region with increasing J. Similarly, at a perturbation frequency of 8·60 Hz, initially stable waves become unstable as they travel downstream. Corresponding to this, the circles pass from the stable region to the unstable region with increasing J. This narrows down the uncertainty in positioning the stability boundary.

A comparison of this experimentally determined stability boundary with Hazel's (1972) numerical studies shows both to have the same characteristics.

The shifting of the stability boundary to the left appears to be reasonable for two reasons.

(i) The effect of the density scale. Hazel (1972) showed that the stability boundary coincides with the line $J = R\alpha$ for small values of J (his figure 8*b*). The line $J = R\alpha$ shifts to the left as R increases. This implies that the left branch of the stability boundary also shifts to the left. However, the line $J = R\alpha$ deviates from the stability boundary (Hazel's figure 8*a*) for larger values of J. More information is needed before drawing the same conclusion as for the small J values.

(ii) The boundary effect. The stability boundary (solid lines in figure 12) was derived for an unconfined flow field by Hazel (1972, figure 8*a*). As the channel boundary moves into 5·08 cm above and below the interface, the stability boundary is affected such that the longer wavelengths (small α) are destabilized while the shorter wavelengths (larger α) become more stable. As a result, both the left- and right-hand branch of the stability boundary move to the left.

In the hope of understanding better the many regions defined by Hazel's figure 8(*b*), the results of Scotti & Corcos have been plotted in figure 13 together with the results of this investigation for small values of J. The two investigations appear to be comparable as both use the shear-layer thickness as the vertical length scale and both evaluate the Richardson number at the interface. It is important, however, to bear in mind the differences.

(i) Scotti & Corcos computed the wavenumber $\beta_i = f/c = f/\overline{U}$, where f is the frequency, c is the phase speed and $\overline{U}$ *is the mean stream velocity*. We obtained the wavenumber by direct measurement of the wavelength. Scotti & Corcos had a perturbation frequency ranging between 20 and 165·7 Hz while our range was 0·476–10·4 Hz.

(ii) Scotti & Corcos replaced the density gradient with the temperature gradient and used the linear relation between temperature and density. We obtained the density distribution by integrating the diffusion equation across the interface.

(iii) Scotti & Corcos had vertical scales for the flow field such that $\delta_u/\delta_t \sim 1$, where δ_u and δ_t are characteristic thicknesses of the velocity and temperature profiles. In our experiment the viscous region was approximately 15 times larger than the scale of the salinity diffusion layer.

(iv) Scotti & Corcos measured the temperature fluctuations, which are related to the change in wave potential energy in the stream direction. In our experiment the stability criteria were determined by direct measurements of the streamwise rate of growth (see figure 4 for example) or decay of the velocity fluctuations.

(v) Scotti & Corcos had typical density variations of 8 % across the interface, violating the Boussinesq approximation $\rho_1 \sim \rho_2 = \rho$. In our experiment the maximum density change was 0·65 %.

(vi) The viscosity change due to the diffusion and radiation of heat across the interfacial region may not have been negligible in the experiments of Scotti &

Corcos. In our experiments the temperature was kept constant, in an air-conditioned laboratory.

In figure 13 the open symbols again indicate growth and the solid symbols indicate decay. Data points below $J = 0{\cdot}8$ are from figure 19 and table 1 of Scotti & Corcos (1972). Data points above $J = 0{\cdot}8$ are from figure 12 of this investigation. Solid lines are the neutral curve and stability boundary of Hazel (1972, figure 8*b*) for hyperbolic tangent profiles. The dashed line is the neutral curve of Hazel (1972, figure 12) for error-function profiles. It is clear that much work is needed to close the big gap left by these two investigations.

It is a pleasure to express my sincere thanks for the help and encouragement of Dr F. K. Browand, who was my supervisor during the time when much of this work was completed. Thanks also go to Dr Rush E. Elkins, III, who helped to smooth the writing of this manuscript. This work was supported by the National Science Foundation through Research Grant GK-4609.

REFERENCES

Drazin, P. C. & Howard, L. N. 1966 *Adv. in Appl. Mech.* **9**, 1.
Fabula, A. C. 1967 *Proc. of International Symposium on Hot-Wire Anemometry, University of Maryland.*
Gibson, C. H. & Schwarz, W. H. 1963 *J. Fluid Mech.* **16**, 357.
Hazel, P. 1972 *J. Fluid Mech.* **51**, 39.
Hinze, J. O. 1959 *Turbulence.* McGraw-Hill.
Howard, L. N. 1961 *J. Fluid Mech.* **10**, 509.
Klebanoff, P. S., Tidstrom, K. D. & Sargent, L. M. 1962 *J. Fluid Mech.* **12**, 1.
Kovasznay, L. S. G. 1949 *Proc. Roy. Soc.* A **198**, 174.
Lock, R. C. 1951 *Quart. J. Appl. Math.* **4**, 42.
Miles, J. W. 1961 *J. Fluid Mech.* **10**, 496.
Roshko, A. 1954 *N.A.C.A. Rep.* no. 1191.
Scotti, R. S. & Corcos, G. M. 1972 *J. Fluid Mech.* **52**, 499.
Taylor, G. I. 1931 *Proc. Roy. Soc.* A **132**, 499.
Thorpe, S. A. 1969 *J. Fluid Mech.* **36**, 673.
Thorpe, S. A. 1971 *J. Fluid Mech.* **46**, 299.
Tritton, D. J. 1971 *J. Fluid Mech.* **45**, 203.

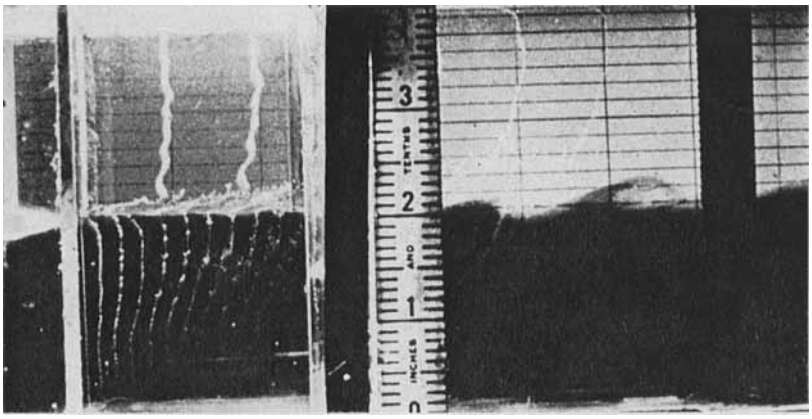

FIGURE 2. Wave breaking at interface; white lines are hydrogen bubbles.

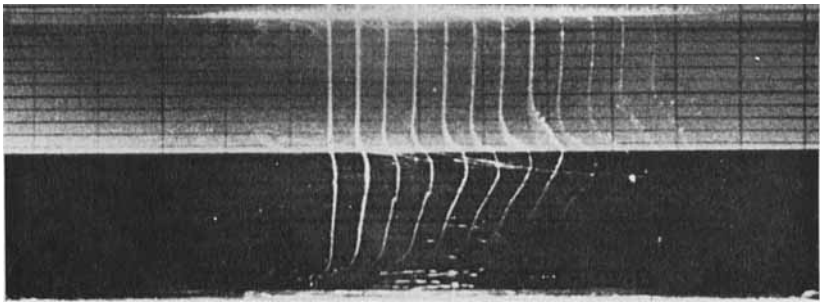

FIGURE 3. Flow condition at which the perturbations are introduced near the interface.

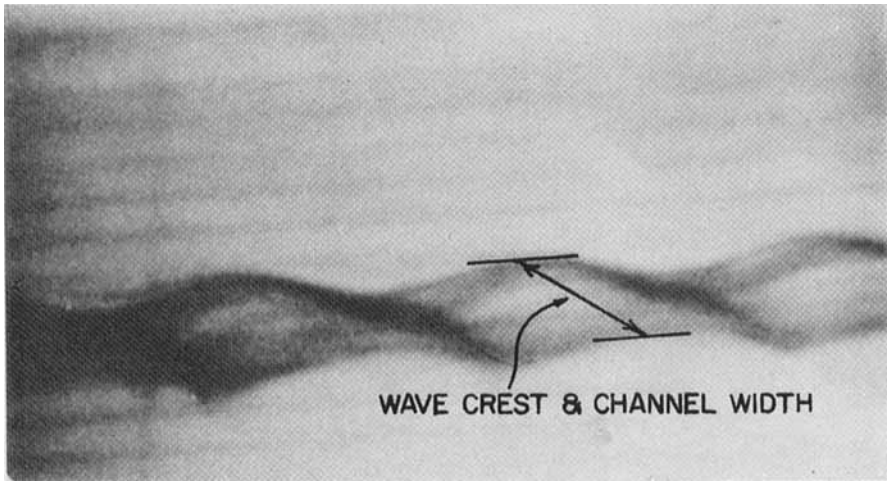

FIGURE 5. Interfacial waves with artificial excitation; only interface is dyed.